*promoting access to White Rose research papers*

**Universities of Leeds, Sheffield and York**
**http://eprints.whiterose.ac.uk/**

This is an author produced version of a paper published in **Acta Materialia**

White Rose Research Online URL for this paper:

http://eprints.whiterose.ac.uk/id/eprint/78182

**Paper:**
Castle, EG, Mullis, AM and Cochrane, RF (2013) *Evidence for an extensive, undercooling-mediated transition in growth orientation, and novel dendritic seaweed microstructures in Cu-8.9 wt.% Ni.* Acta Materialia, 66. 378 - 387 (10). ISSN 1359-6454

http://dx.doi.org/10.1016/j.actamat.2013.11.027

*White Rose Research Online*
*eprints@whiterose.ac.uk*

**Evidence for an extensive, undercooling-mediated transition in growth orientation, and novel dendritic seaweed microstructures in Cu-8.9wt%Ni**

Elinor G. Castle[a], Andrew M. Mullis[b], Robert F. Cochrane[c]

[a]Institute of Materials Research, University of Leeds, Leeds LS2 9JT, UK.
pm07egc@leeds.ac.uk

[b]Institute of Materials Research, University of Leeds, Leeds LS2 9JT, UK.
A.M.Mullis@leeds.ac.uk

[c]Institute of Materials Research, University of Leeds, Leeds LS2 9JT, UK.
R.F.Cochrane@leeds.ac.uk

**Corresponding author:**

Elinor Castle. IMR, School of Process, Environmental and Materials Engineering, Engineering building, University of Leeds, Leeds, LS2 9JT, UK. pm07egc@leeds.ac.uk. +44(0)113 343 2391 or +44(0)7891519694.

**Suggested reviewers:**

**Doug Matson,**

Vice Chair, Department of Mechanical Engineering, Tufts University, Medford, MA 02155, douglas.matson@tufts.edu

**Bill Hofmeister**,

Director, Center for Laser Applications, Materials Science and Engineering, University of Tennessee Space Institute, Tullahoma, TN 37388-9700. hof@utsi.edu

**Peter Schumacher,**

Managing Director, Austrian Foundry Research Institute, Parkstrasse 21, 8700 Leoben, Austria, giesskd@mu-leoben.at

**Bingbo Wei,**

Vice president, Northwestern Polytechical University, School of Natural and Applied Sciences, Northwestern Polytechnical University, Xi'an city, P.R. China, bbwei@nwpu.edu.cn

**Abstract**

Within the context of rapid solidification, a melt-fluxing technique has been employed to study the microstructural development and velocity-undercooling relationship of a Cu-8.9wt%Ni alloy. A number of microstructural transitions have been observed up to undercoolings of 235 K. At the lowest undercoolings, single grain, <100> type dendritic structures are observed, which give way to a recrystallised grain structure as undercooling is increased. At intermediate undercoolings, twinned dendritic samples exhibiting features of mixed orientation are reported. Within this range, dominant <100> character is evidenced by 8-fold growth at low undercooling whilst <111> character begins to dominate at high undercooling, accompanied by a switch to 6-fold growth. It is believed that this range of undercooling represents an extended transition between fully <100> oriented growth at low undercooling and fully <111> oriented growth at high undercooling. It is suggested that an observed positive break in the velocity-undercooling relationship at high undercooling is therefore coincident with the transition to fully <111> growth, though this could not be confirmed microstructurally. The existence of competing anisotropies in the growth directions at intermediate undercoolings appears to be giving rise to a novel form of the dendritic seaweed structure, characterised by its containment within a diverging split primary dendrite branch. In addition, at the highest undercoolings achieved, an equiaxed-to-elongated grain structure is observed, in which an underlying dendritic seaweed substructure exists. We suggest that this structure may be an intermediate in the spontaneous grain refinement phenomenon, in which case dendritic seaweed appears to play some part.

**Keywords:** Rapid solidification, anisotropy, orientation relationship, undercooling, spontaneous grain refinement

## 1. Introduction

The rapid solidification of metallic melts is a subject of enduring interest within the metallurgical community. Such non-equilibrium processing conditions give rise to a number of metastable phenomena, many of which will offer substantial engineering advantages once the fundamental processes behind their formation can be understood and subsequently manipulated. Undercooling methods promote rapid solidification in spite of their slow-cooling nature, as a large driving force for solidification is created from the difference in Gibbs' free energy between the solid and the metastable liquid states. Such techniques offer direct analysis of the physical processes occurring during the rapid solidification of metals, and also provide full control over process parameters, such as temperature and cooling rate. Developments in microstructure with increasing undercooling and, by extension, solidification velocity, thus provide experimental evidence for the fundamental mechanisms at play during rapid solidification.

A number microstructural changes have been observed in several different metal and alloy systems with increasing undercooling, including the observation of an abrupt transition from a course columnar to a fine-grained equiaxed structure at a characteristic undercooling, $\Delta T^*$. Spontaneous grain refinement was first reported in pure Ni in 1959 by J. L. Walker [1], and has since been observed in a number of metallic systems, including Cu-O [2], Cu-Sn [3], Ge [4] and Fe-Co [5]. Fine grained metals have long been appreciated for their improved properties and are conventionally produced extrinsically by mechanical or chemical means. By contrast, grain refinement in rapidly solidified metals is intrinsic to the solidification process, making rapid solidification processing an attractive alternative.

However, the fundamental origins of spontaneous grain refinement in the deeply undercooled regime are not yet fully understood and remain a subject of debate. Walker initially proposed

that copious nucleation, as a result of cavitation in the melt ahead of the solid-liquid interface, could yield refined microstructures. However, many alloy systems, such as Ni-Cu [6] and Fe-Ni [7], also display a second region of equiaxed grains at lower undercoolings. This stabilisation of columnar growth at intermediate undercoolings cannot be accounted for by Walkers' theory alone, and a number of alternative theories have since been put forward. These have included: partial remelting of secondary and tertiary dendrite branches [8], dendrite fragmentation [9, 10], and a dendrite coarsening, remelting and recrystallisation mechanism driven by excess solute trapping [2]. However, the most widely accepted model is that of Schwarz et al. [11] who proposed a surface energy driven remelting and fragmentation process, based on the stability analysis of Karma [12]. Their model accounts for the occurrence of both regions of grain refinement and appears to be in close agreement with experimental evidence. However, the theoretical basis for the Karma model was not published until several years after the publication of the Schwarz model and has since been brought into question [13].

Mullis et al. later proposed that grain refinement may result from a transition in growth mode, from dendritic to dendritic seaweed, at $\Delta T^*$ [14]. It is proposed that, above $\Delta T^*$, dendrite growth becomes unstable, with repeated tip splitting leading to the formation of seaweed. Their model is an attractive alternative to the Schwarz model since it can account for an apparent coincidence of $\Delta T^*$ with both a discontinuous break in the velocity-undercooling relationship [3, 15, 16], and the observation of a change in growth front morphology [17]. Their model is further supported by experimental observations of a 'trapped-in' seaweed-like structure in samples of highly undercooled pure Cu [18].

Dendritic seaweed is an inherently unstable structure which is likely to partially remelt post-recalescence, forming many solid islands on which new, fine grains could nucleate. It is a structure of low symmetry and low anisotropy, with no strong preference in the growth

direction and has thus been shown to arise in situations where competing anisotropies in the growth direction become comparable in strength. For example, in 1986 [19] it was shown that, in the anisotropic crystal system of aqueous $NH_4Cl$, undercooling-mediated changes in the relative strengths of anisotropy of the <100> and <110> growth directions were occurring. When the two anisotropies became equal, a 'dendrite of oscillatory type' appeared, characterised by irregularly splitting tips which do not follow a preferred orientation and whose growth is finally halted by impingement on neighbouring branches. The study showed that in a 'free' dendrite system, dendrites do not necessarily grow in crystallographic directions and erratic patterns can be formed. In fact the co-existence of mixed secondary branches which are both symmetrical and non-symmetrical, and either periodic or erratic, were observed on the same dendrite. Further studies into the $NH_4Cl$-$H_2O$ system show that developing dendrites will transition from slow <100> to fast <111> type growth when there is a significant drop in interface temperature [20]. Similar observations have been made in Cu-Sn alloys [21], wherein a transition from <111> to <100> growth was observed above a critical value of undercooling, $\Delta T'$. Note that, given two competing anisotropies where one dominates at low growth velocity (capillarity) and one dominates at high velocity (kinetic), a second region of dendrite stability will naturally occur beyond the region of seaweed growth.

Such transitions provide clear indications for the existence of competing anisotropies in the growth direction, the relative strengths of which appear to vary with the degree of undercooling (solidification velocity). Furthermore, these conditions may favour the growth of the seaweed morphology and, potentially, other novel or mixed microstructures, which may provide key evidence for the fundamental origins of spontaneous grain refinement. The present report investigates the velocity-undercooling relationship of a Cu-8.9wt%Ni alloy, using a glass encasement (fluxing) technique to undercool samples by up to 235 K. In order to help illuminate the possible origins of spontaneous grain refinement in this alloy, detailed

microstructural and X-ray texture analysis of the undercooled samples has been performed so as to identify any transitions in preferred growth orientation or dendrite morphology with increasing undercooling.

## 2. Material and methods

High purity 99.999 %, metals basis Cu and Ni powders, of 100 and 120 mesh respectively, were weighed and mixed to a Cu-10at%Ni concentration and compacted into pellets. These were subsequently arc-melted together under an inert argon atmosphere, ensuring complete mixing of the components after three re-melts. X-ray diffraction patterns obtained from the resulting slug exhibit sharp peaks and a steadily increasing background Cu fluorescence with angle $2\theta^{o}$. Any inhomogeneities in the alloy composition would contribute to peak broadening, due to the resultant variations in lattice parameter, and may result in sharp increases in Cu-fluorescence. Hence it was determined that a sufficient degree of homogeneity had been achieved through this technique, and that different samples taken from the alloy slug were therefore of comparable composition. The final composition was established[1] to be Cu-8.9wt%Ni using X-ray Fluorescence (XRF) analysis. The 2.04wt% material loss during arc melting can account for this alteration in composition of the final slug. Additional light element combustion analysis (LECO®) was also performed in order to determine residual oxygen concentration. Both XRD and LECO® analysis indicate the presence of oxides in the sample, with a confirmed total oxygen content of 0.237 wt%. However, the relatively low oxygen content was not considered to be a concern, since oxides tend to partition out of the melt and into the glass flux during successive fluxing cycles.

[1] XRF and LECO® analysis performed by LSM Analytical Services

Spherical samples of 5-7 mm in diameter were heated in fused silica crucibles by induction heating of a graphite susceptor, contained within an alumina radiation shield. In order to reduce the number of potential heterogeneous nucleation sites, the droplets were isolated from the crucible walls by suspension in an 40% $Na_2SiO_3$ – 60% $B_2O_3$ glass flux, which was previously mixed and dewatered at 1073 K for 30 min in a high temperature furnace. The undercooling experiments were carried out within a stainless steel vacuum chamber, evacuated to $10^{-5}$ mbar and backfilled to 500 mbar with $N_2$. This contained a glass viewing window, which allowed visibility of the sample through slots cut into the susceptor and alumina shield. High speed digital imaging (up to 15 000 fps) of the sample was therefore permitted, allowing *in situ* growth velocity measurements of the recalescence front. Samples were subjected to repeated heating and cooling cycles, in which they were superheated to around 130 K above the liquidus temperature (to 1553 K) and held at this temperature for 15 minutes, ensuring complete melting and encasement of the sample and removal of gas bubbles from the flux. Samples were then slow-cooled through the liquidus at an average rate of 10 K/min. Temperature was monitored by means of an r-type thermocouple positioned at the base of the crucible.

Solidification was allowed to nucleate spontaneously (as opposed to inducing nucleation through the use of a trigger needle) as this was found to occur naturally over a wide range of undercoolings and ensures that solidification proceeds from a single nucleation point, simplifying post-solidification analysis.

Where possible, the nucleation site and any significant features evident on the surface of the undercooled droplets were imaged using SEM or light microscopy. Optical microscopy, in bright-field, dark-field and differential-interference contrast (DIC) modes was performed using an Olympus BX51 microscope, fitted with a Carl Zeiss AxioCam MRc5 camera. In order to compensate for the shallow depth of field of the light microscope when imaging the

spherical sample surface, a stack of through-focused images was obtained of each feature and blended together using Adobe® Photoshop® Elements software. To track the development of microstructure over large areas, a Carl Zeiss EVO MA15 SEM, equipped with SmartStitch® acquisition and image stitching software, was used to map high resolution montages of the droplet surface topographies. Droplets were then mounted in Bakelite and sectioned using a diamond wafering blade. Since growth proceeds radially outwards from the nucleation point, droplets with evident nucleation points could be sectioned with a well-defined orientation relative to their growth direction. To assess the interior microstructure of the droplets they were then polished and etched using an aqueous solution of ammonium persulphate, and imaged using optical microscopy. A selection of droplets were then subjected to texture analysis through XRD pole figure plots, generated by a Phillips/PanAlytical diffractometer (Cu $K_\alpha$ radiation) equipped with a texture stage. Pole figures were subsequently interpreted using PanAlytical X-Pert Texture software.

## 3. Results and discussion

The velocity-undercooling curve for the Cu-8.9wt%Ni alloy studied is shown in figure 1. Error bars for velocity calculations are estimated to be ±20 %, taking into account the human and instrumental error associated with measuring the progression of the growth front from frame to frame. Evidently, the error rises as the growth velocity, and therefore distance travelled per frame, increases. The growth velocity initially increases relatively slowly with undercooling, following the power law trend $V \propto \Delta T^{1.92}$. At around $\Delta T$ = 200 K, a break in this trend is observed, as a steep increase in growth velocity occurs, with the exponent of $\Delta T$ increasing to 6.50. This is confirmed by a log-log plot of the data, which demonstrates two distinct linear trends. Velocity-undercooling relationships of this type have been previously reported in the Ni-Cu system by Algoso et al. [22] whilst investigating the Ivantsov solution

with marginal stability arguments (IMS) [23]. However, in this instance, plateaus in the velocity-undercooling relationship were observed on either side of the sharp increase. Algoso et al. attributed the first velocity plateau to the addition of 5 and 10 at% Cu solute, since pure Ni does not exhibit such a plateau, whilst the second plateau is thought to be due to residual oxygen in the system. Based on this, a plateau at high undercoolings may not have been observed, either due to the low residual oxygen concentration in the alloy, or because it exits beyond the range of undercooling achieved in this investigation. Further to this, a plateau prior to the transition is not observed, though this is difficult to confirm from the data collected due to the degree of scatter displayed.

A break in the velocity-undercooling curve is indicative of a growth transition at this undercooling. Dragnevski et. al. [21] observed a positive break in the V-ΔT relationship for Cu-Sn alloys and found that it was coincident with an abrupt transition from <111> growth at intermediate undercooling to <100> growth at high undercooling. For all compositions tested they concluded that the two power law trends observed related to the two growth modes (either <111> or <100>) and that, at a specified undercooling, the fastest growing mode would dominate.

Microstructural analysis was performed on Cu-Ni droplets solidified over the full range of undercooling in order to investigate whether such a transition had occurred. This revealed a yet more complicated sequence of growth transitions, the extent of which are summarised in figure 1.

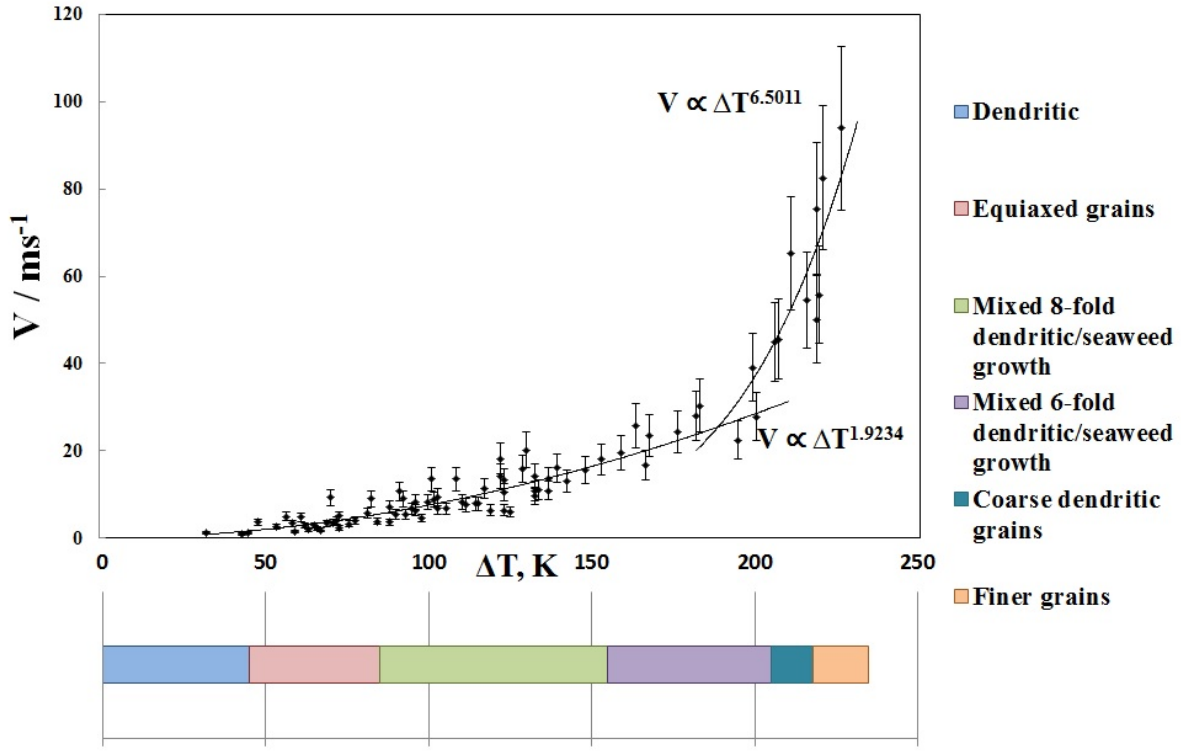


**Figure 1.** Growth velocity (V) as a function of undercooling (ΔT) and a summary of the growth transitions observed with increasing undercooling in Cu-8.9wt%Ni.

### 3.1. Single grain dendritic up to ΔT = 45 K

Beginning with the smallest undercoolings, droplets solidified up to around 45 K below the liquidus temperature comprise of one large grain, consisting of a coarse dendritic structure, an example of which is presented in figure 2, showing a DIC micrograph of a droplet undercooled by 35 K. Orthogonality is observed in the dendrites solidified in this range of undercooling. This is typical of an FCC alloy which has solidified along the more usual <100> direction.

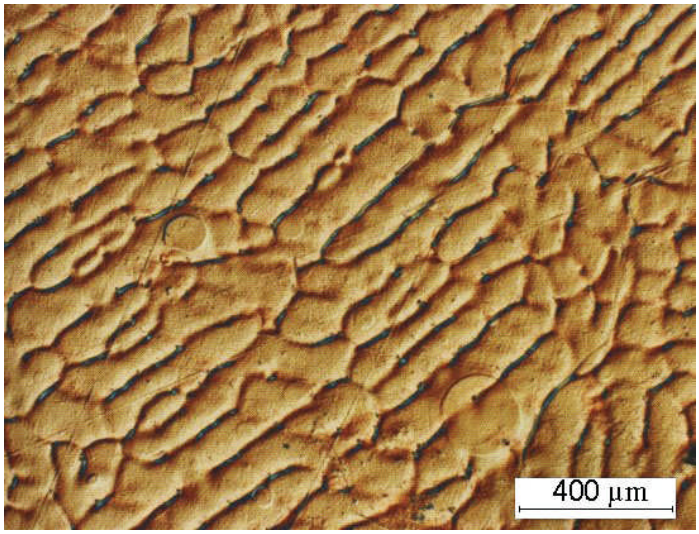


**Figure 2.** Micrograph of randomly-sectioned Cu-8.9wt%Ni droplet undercooled by $\Delta T = 35$ K, taken in DIC mode to show coarse dendritic structure.

### 3.2. Equiaxed grains between 45 K ≤ ΔT ≤ 85 K

In the undercooling region 45 K ≤ ΔT ≤ 85 K, a coarse equiaxed grain structure is observed, in which there appear to be large parent grains consisting of smaller sub-grains. This is indicated by the difference in contrast between large areas, as shown in the top image of figure 3(a) - an optical micrograph of a sectioned, polished and etched sample which has been undercooled by $\Delta T = 65$ K prior to solidification. The existence of curved grain boundaries, as indicated by the arrows, suggests that grain boundary migration has taken place, whilst the DIC micrograph of the same area (bottom image in figure 3(a)) appears to show that the coarse dendritic segregation pattern extends across the grain boundaries. Figure 3(b) shows the {200} pole figure plot taken from a randomly-oriented section of this sample. This exhibits only three sharp poles related to one another through $90^{o}$ angles, confirming that the dendritic substructure is continuous throughout. Hence, it is suggested that some post-solidification grain coarsening has occurred, consistent with the recrystallisation mechanism associated with the low undercooling region of grain refinement observed in many alloys.

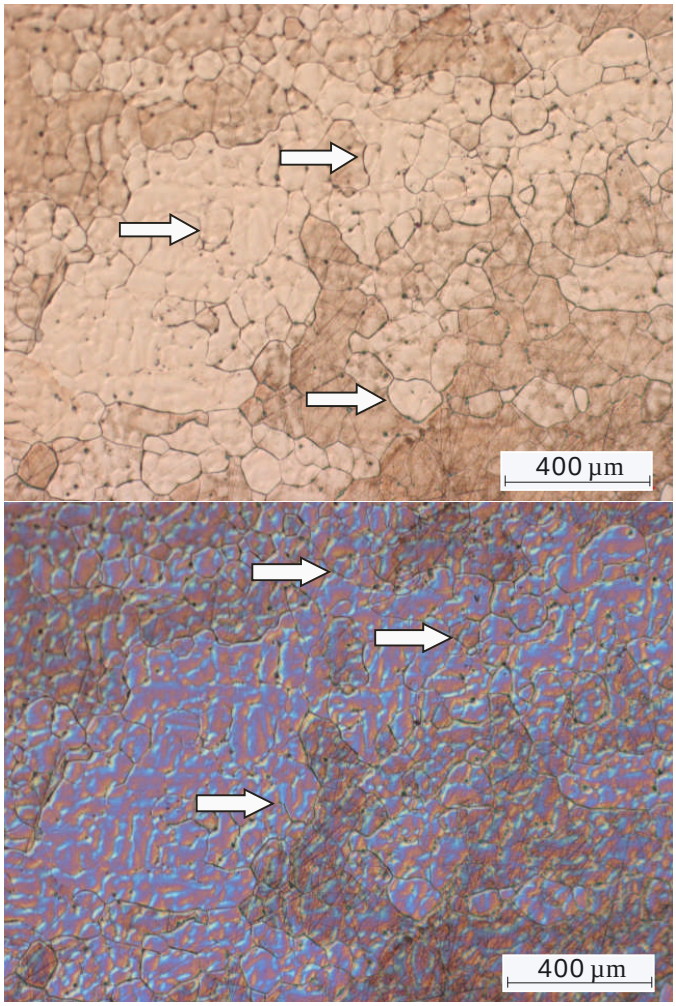


(a)

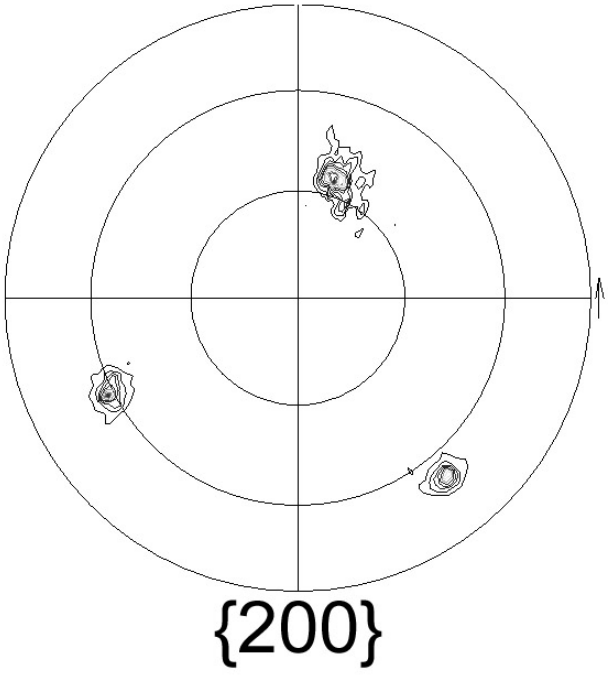

(b)

**Figure 3.** (a) Optical micrograph of Cu-8.9wt%Ni undercooled by ΔT = 65 K prior to nucleation in: bright field mode (top) where arrows show the positions of curved grain boundaries, and DIC mode (bottom) revealing a dendritic substructure which appears to cross the grain boundaries, as indicated by the arrows. The corresponding {200} pole figure is shown in (b).

### 3.3. 8-fold, mixed-orientation dendritic growth and seaweed branches between 85 K ≤ ΔT ≤ 155 K

Above 85 K undercooling, a transition back to dendritic growth is observed. Up to an undercooling of around ΔT = 155 K, the nucleation points observed on the surface of the samples exhibit near 8-fold growth patterns and mixed-morphology dendrites are observed. Figure 4(a) shows an optical microscope image of a nucleation point observed on the surface of a droplet undercooled by 139 K, which is a typical example of droplets undercooled in this range. Further development of these dendrites can be observed in the SEM secondary electron (SE) image shown in figure 4(b). A split primary dendrite branch can be seen (feature 1) exhibiting orthogonal secondary branches, whilst at 90$^{o}$ to this, feature 2 shows a primary branch whose secondary arms appear to have grown at an angle which is indicative of either <110> or <111> type growth.

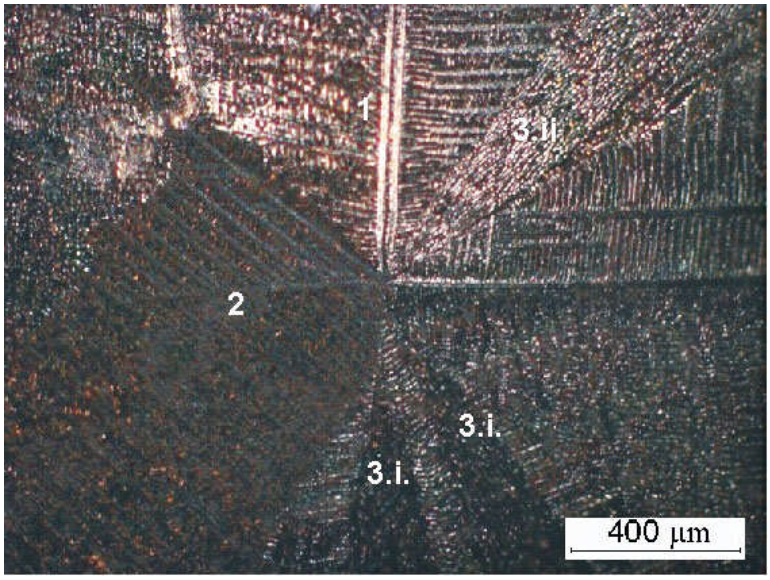

(a)

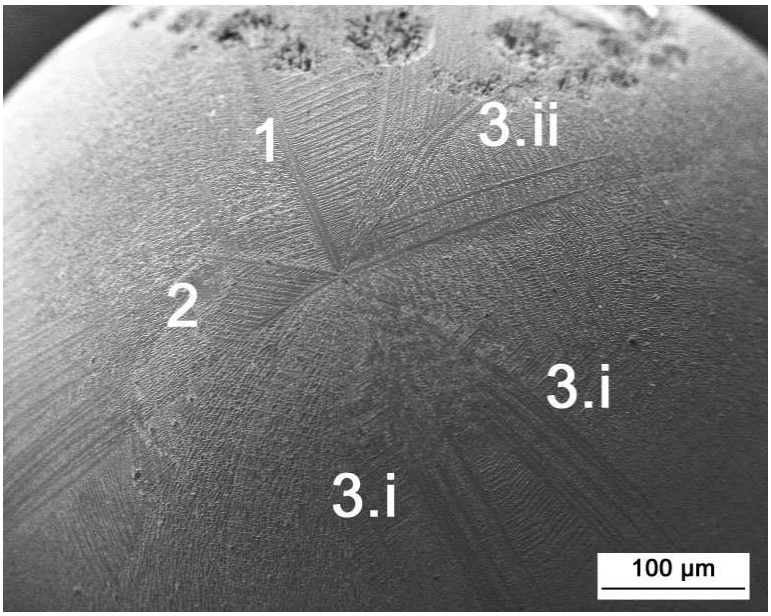


(b)

**Figure 4.** (a) Optical through-focused micrograph and (b) SEM secondary electron image of the surface topography of a Cu-8.9wt%Ni droplet undercooled by $\Delta T = 139$ K exhibiting an 8-fold nucleation pattern. Numbered features indicate (1) split primary dendrite trunk with orthogonal secondary branches (2) primary dendrite trunk with non-orthogonal <111> type branches (3) three seaweed branch structures of type (i) and (ii).

### 3.3.1 Dendritic seaweed branches observed between 85 K ≤ ΔT ≤ 205 K

Features labelled with a '3' in Figure 4 indicate the positions of a novel dendritic seaweed-like structure, which have been observed to arise in all intermediate-undercooling samples up to around $\Delta T = 205$ K. These structures have the appearance of a region of dendritic seaweed which is bound by dendrites and seems to evolve from a diverging split primary branch, whose inner secondary branches have undergone multiple tip-splitting. In some cases, orthogonal outer secondary branches are observed to have grown from the split primary branches. In these cases, the seaweed growth is observed to terminate in an array of parallel <100> type dendrites. The $\Delta T = 139$ K droplet images show two instances of this type of

seaweed structure (3.i.) which have grown adjacent to one another. However, in some instances, no outer secondary branches are observed, as seen in the seaweed structure shown to the top right hand corner of figure 4(a) (feature 3.ii). In this case, the seaweed structure appears to eventually break down via the growth of <111> type dendrites, which can be seen in the SEM image in (b).

### 3.3.2 Texture analysis of the 8-fold growth regime

Pole figure plots of the {200}, {220} and {111} projections, taken from a section parallel to the growth direction of this sample ($\Delta T = 139$ K), are shown in figure 5. Whilst the sharp poles indicate a preference in growth orientation, the absence of any pole from the centre of every plot, possibly as a result of slightly off-axis sectioning, renders the growth orientation difficult to conclude. Plotting the pole figure data on a log scale (bottom images of figure 5) reveals a large amount of additional texture on both the {200} and {111} pole figures. It is unclear why this may be, but we suggest that this may relate to the two forms of seaweed structure observed in this sample. The seaweed may have grown in a general crystallographic direction, since it is bound by oriented outer dendrite branches, yet would otherwise have developed without any preference in growth orientation. Hence, the texture observed in the {200} pole figure may relate to a seaweed branch (or branches) growing with an overall <100> orientation, but where repeated bending and splitting of the seaweed tips has resulted in the {100} planes becoming misoriented with respect to one another, resulting in weak {100} reflections from a broad range of $\Phi$ and $\Psi$ angles. It is suggested that such texture has arisen from the type of seaweed branches, identified as 3.i in figure 4, which have orthogonal outer secondary branches and which terminate in <100> type dendritic arrays. Conversely, the texture observed on the {111} pole figure plot is suggested to arise from the second type of seaweed branch identified in this sample (feature 3.ii), which terminates in a <111> type dendritic array.

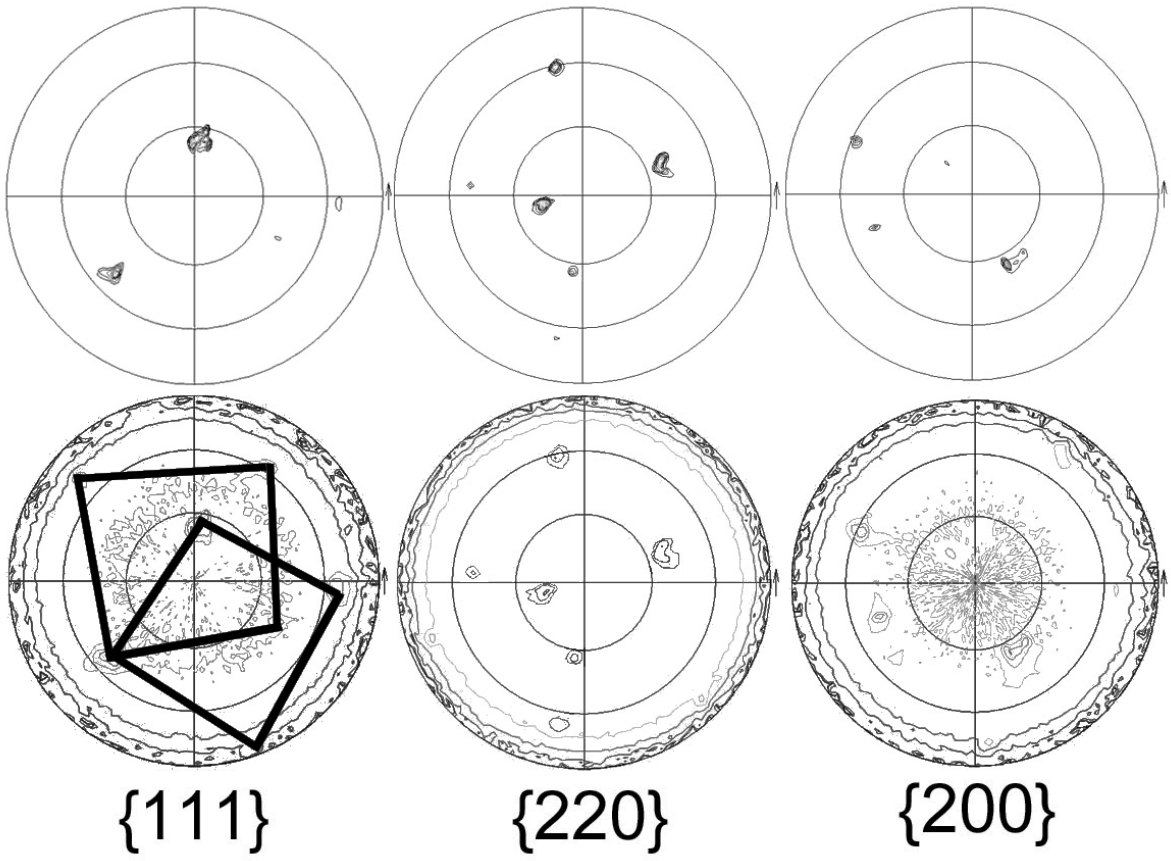


**Figure 5.** (Top) Showing pole figures corresponding to the ΔT = 139 K droplet shown in figure 6, (bottom) equivalent pole figures with intensity plotted on a log scale, the {111} plot showing two sets of poles with one pole shared between them, indicating twinned growth.

All three log-scale pole figures exhibit the presence of a further set of weak poles, indicating the existence of a second grain. By using X'pert texture analysis software to measure the angular relationship between these, it becomes evident from the {111} plot that there are two groups of poles related to one another via common angles of 72 deg, 53 min or 109 deg, 47 min, as indicated on the log{111} pole figure. The existence of a shared pole between the two sets, which is not the strongest peak present, is indicative of twinned growth in one of the secondary growth directions. As growth proceeded from a single nucleation point, twinning appears to have occurred during the growth of one of the secondary dendrite arms, giving rise to a second, orientationally-related crystal

### 3.4. 6-fold mixed-orientation dendritic growth and seaweed branches between 155 K ≤ ΔT ≤ 205 K

Above an undercooling of ΔT ≈ 155 K a transition from 8-fold to 6-fold growth is observed, accompanied by a switch to a dominant <111> growth orientation. As with samples observed in the 8-fold regime, features of mixed growth orientation are again present. Figure 6(a) (left image) shows a micrograph of the 6-fold nucleation point on the surface of a sample which has been undercooled by ΔT = 161 K prior to solidification. The feature labelled as '1' indicates a primary dendrite branch whose secondary arms unusually grow orthogonal on one side and non-orthogonal on the opposite side. To the right of this, a neighbouring primary branch displaying strong <111> type growth features is observed, whilst to the left of it is a seaweed branch (feature 2) of <100> type as described previously. The growth progress of this branch was tracked using montage software on the SEM. This image demonstrates in high resolution the unique features of this structure. From the nucleation point (bottom right of image) a primary branch appears to have split soon after its formation. Secondary arms on the inside of this split are then observed to have periodically grown and bent to become near parallel to the primary branch. The tips have then undergone multiple tip splitting, progressing until their path is obstructed by neighbouring branches. On the outside of the split primary, near-orthogonal secondary arms can be seen. After some distance, the seaweed growth terminates in an array of parallel <100> type dendrites. Once more, along with the observation of a <100> type seaweed branch, additional texture is observed on the {200} pole figure plot only, when intensity is plotted as a log scale.

The associated {111} pole figure plot (log scale) taken from a section parallel to the growth direction, is shown to the right of figure 6(a), whose strongest peak is located close to the centre of the pole figure, confirming a dominant <111> sample orientation. Poles 1, 2, 3, 6 and 7 are all evident on the linear scale pole figure plot, whereas poles 4 and 5 appear only on

the log(intensity) plot. One complete set of poles is given by poles 1 to 4, who all share common angles of either 72$^{o}$ or 109$^{o}$ with each other. Further investigations into the angular relationship between the remaining poles reveal a possible triple-twin relationship. Poles 4, 5 and 6 can all be related to one another through common angles, as can poles 6, 2 and 7. Hence there appear to be three grains, with each grain sharing a pole with each of the other two (either pole 2, 4 or 6). The fourth poles of the additional two grains do not appear on the pole figure, it is possible that these may be situated out of the range of detection at the perimeter of the pole figure (i.e. at 90$^{o}$ Ψ).

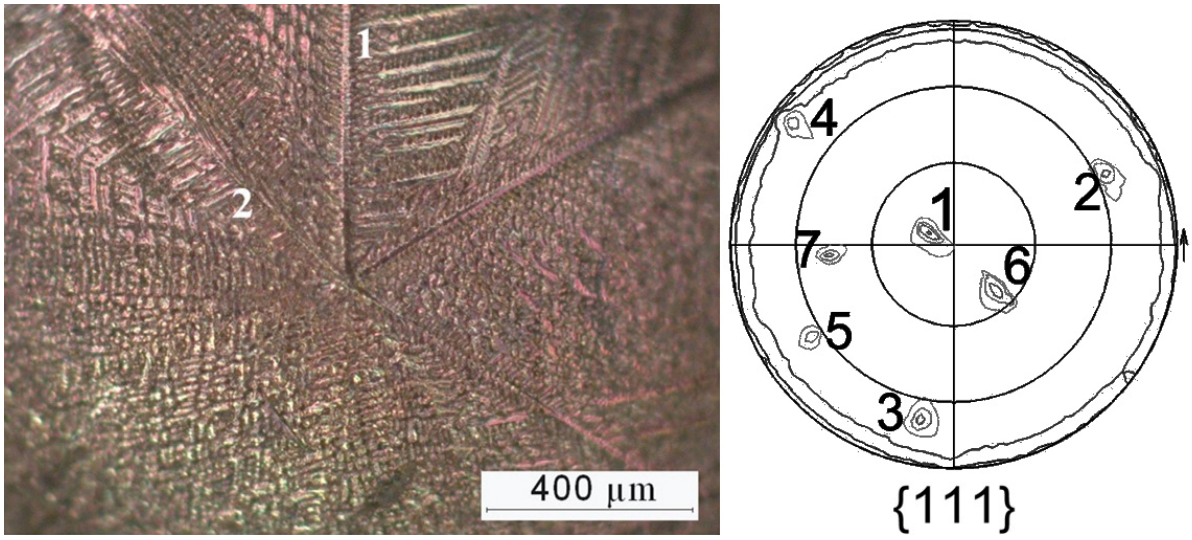


(a)

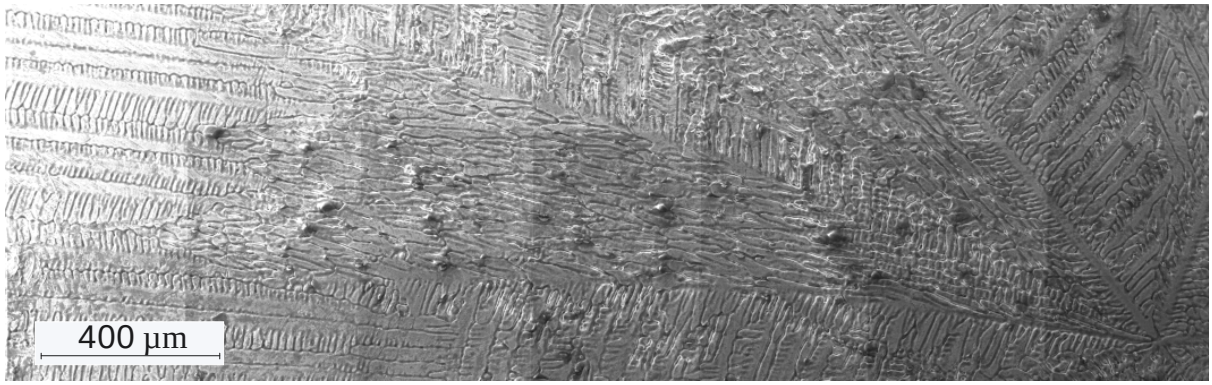


(b)

**Figure 6.** (a) Optical micrograph of the surface topography of a Cu-8.9wt%Ni droplet undercooled by $\Delta T = 161$ K, exhibiting a 6-fold nucleation pattern (left) and corresponding {111} pole figure, with intensity plotted on a log scale (right). Numbered features indicate (1) primary dendrite branch exhibiting both orthogonal and non-orthogonal branches and (2) the branch of dendritic seaweed shown in (b) a montage SEM image of the full seaweed branch, with nucleation point in the bottom, right-hand corner and the seaweed branch growing from right to left.

### 3.5. Coarse dendritic grains between 205 K ≤ ΔT ≤ 220 K

At an undercooling of around $\Delta T = 205$ K, coincident with the break in the V-$\Delta T$ curve, the as-solidified samples undergo a transition to a coarse-grained structure, consisting of a substructure of dendrites of a large variety of morphologies and sizes. Figure 7(a) shows an optical microscope image of the surface topography of a droplet undercooled by $\Delta T = 214$ K. The variety and mixture of dendrites typical of these samples is evident in this image, with the coexistence of both fine and coarse dendrites and with secondary arms of mixed orientation. In some cases, neighbouring secondary arms are observed to have grown in separate orientations relative to one another.

Figure 7(b) shows a DIC image (left) of the interior microstructure of the droplet, after random sectioning (since the nucleation point is no longer present). This reveals coarse grains, whose underlying dendritic substructure appears to be discontinuous across the grain boundaries. This is confirmed by the corresponding {111} pole figure (right) taken from this section, which shows four strong poles located close to $60^{o}$ Ψ. There is a common angle between these poles of $72^{o}$ and hence these belong to one grain. In addition, there are several additional poles which cannot be related to these four poles via $72^{o}$ or $109^{o}$ angles. These must relate to neighbouring grains, between which it seems no orientational relationship exists.

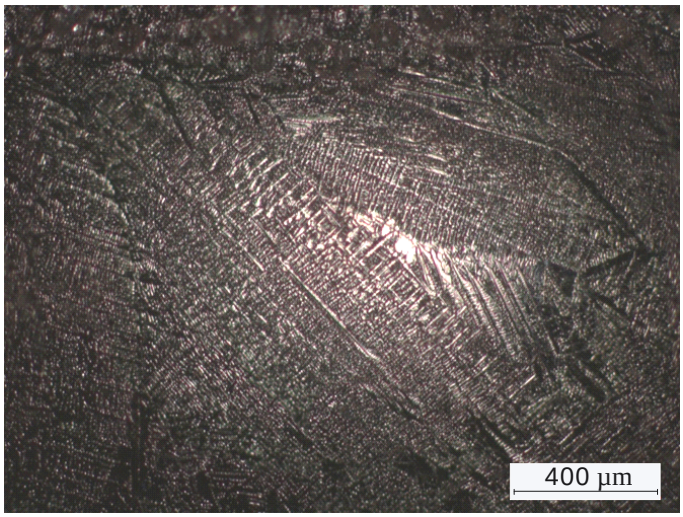


(a)

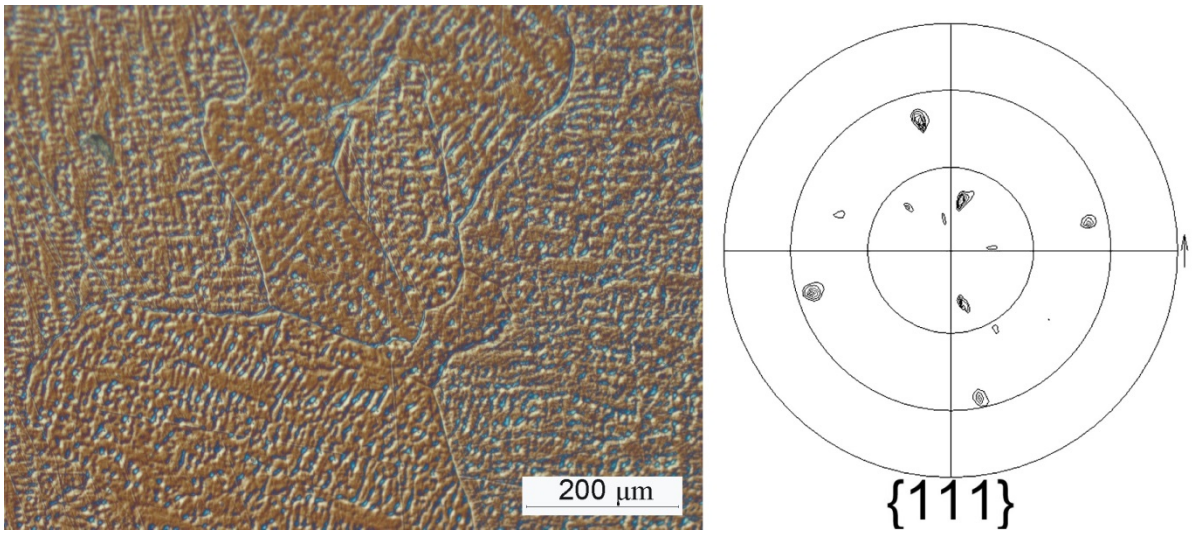


(b)

**Figure 7.** Cu-8.9wt%Ni sample undercooled by ΔT = 214 K prior to nucleation (a) optical microscope image of the surface topography of the droplet showing an array of dendrites of mixed morphology and size and (b) a DIC micrograph of the of the droplet interior (left) showing coarse grains, whose underlying dendritic substructure appears to be discontinuous between neighbouring grains, and (right) the corresponding {111} pole figure.

### 3.6. Finer grains and underlying dendritic seaweed structure up to 235 K

Finally, up to the highest undercooling achieved ($\Delta T$ = 235 K) a decrease in grain size is observed above undercoolings of around $\Delta T$ = 220 K. Figure 8(a) shows an optical dark-field montage of a randomly sectioned droplet undercooled by $\Delta T$ = 220 K. Some directionality is still present in this droplet, as is evident from the grain structure which appears to transition from equiaxed through to elongated grains from right to left (approx.). The region of high reflection in the centre is due to the large amount of porosity present in this area. The majority of the sample has an underlying dendritic substructure, which in some regions is distinctly seaweed-like, as shown in figure 8(b), a high-contrast image of the region outlined on the montage. Many of the equiaxed grains observed do however appear devoid of any substructure. The inset {111} pole figure in figure 8(a) displays a large number of poles which are mostly confined to one half of the pole figure, suggesting that there are many individual grains present, but that overall directionality is still prevalent.

Though these grains are considerably finer than that of the 205 K $\leq \Delta T \leq$ 220 K range, spontaneous grain refinement is not considered to have occurred, as a global transformation to fine equiaxed grains over the full sample is not observed. It is possible, however, that this structure represents an intermediate stage in the grain refinement process, in which case, dendritic seaweed appears to play an important role.

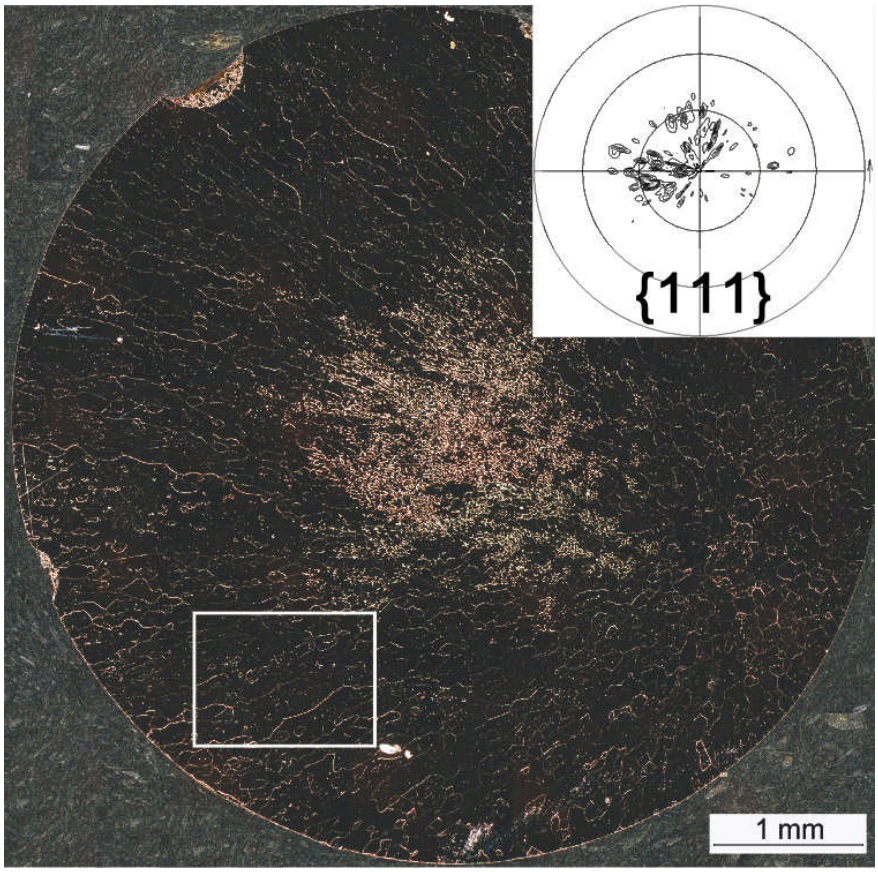


(a)

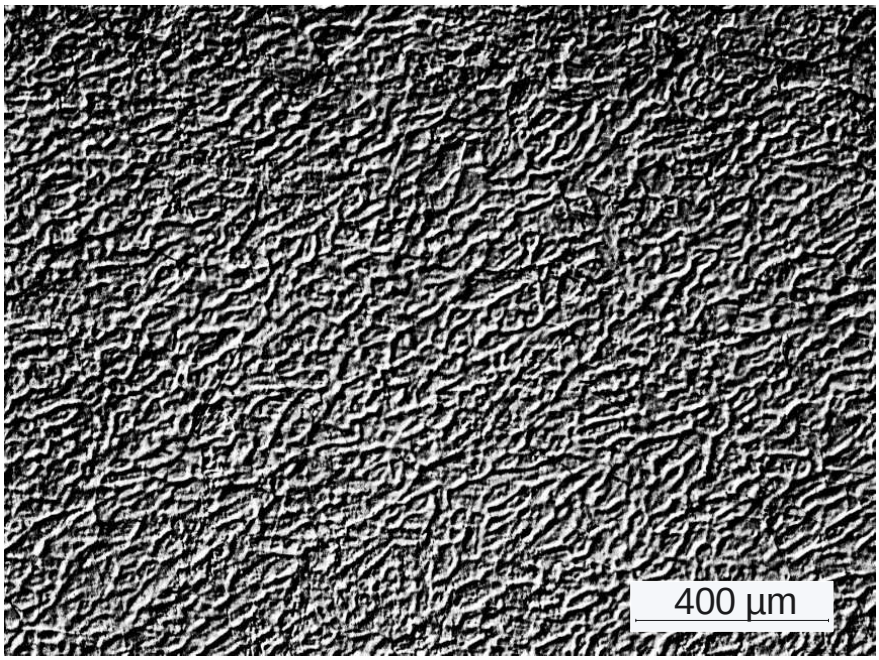


(b)

**Figure 8**. Optical micrographs of a Cu-8.9wt%Ni droplet undercooled by ΔT = 220 K, randomly sectioned and etched, showing (a) dark field montage image of the internal grain structure of the whole droplet and inset {111} pole figure. The area outlined indicates the approximate area depicted in (b) enhanced-contrast DIC micrograph showing the fine dendritic seaweed microstructure observed in this region.

## 4. Further discussion

As seen, at intermediate undercoolings there appears to have been some competition between <100> and <111> oriented growth. This is giving rise to the twin-assisted growth of mixed morphology microstructures and branches of dendritic seaweed. We suggest that what we are observing is a considerably extended transition between fully <100> growth at low undercooling to fully <111> growth at high undercooling. In the transitional zone, we therefore see the growth of dominant <100> character at low undercooling (8-fold growth) which transitions to dominant <111> character at higher undercoolings (6-fold growth). If this is the case, then the positive break in the velocity-undercooling relationship is due to the loss of all intermediate character and the transition to faster, fully <111> growth. However, this is difficult to confirm microstructurally as the original growth structure has been modified via post-solidification processes.

To our knowledge, such an extensive transition between growth modes with respect to the degree of undercooling has not previously been reported. A near analogous transition has been reported by Dantzig et. al. [24] in directionally solidified Al-Zn alloys, in which they observe an extended transition between <100> growth and <110> growth with increasing Zn content. In the intermediate range, referred to as the 'Dendrite Orientation Transition, (DOT)', they find that competition between the differently directed growth anisotropies give rise to textured, seaweed-like structures. This is distinct from the work presented herein, as it

sees abrupt transitions between well-defined morphologies and does not report any significant change in dendrite character within the transitional range of composition.

What is clear is that changes in the anisotropy of the system can have a profound influence on the growth mode and therefore the as-solidified microstructure. Such changes appear to be mediated by the degree of undercooling (or growth velocity) in the Cu-Ni alloy studied, and may be contributing in some way to the spontaneous grain refinement phenomenon. Though we have not seen a full transition to a grain refined structure within the undercooling range achieved, we have observed a possible partially-refined structure in which both fine, equiaxed grains and large elongated grains exist. The original directionality of the sample is still evident, suggesting that a full post-solidification transformation has not occurred. Therefore, the presence of a dendritic seaweed substructure within the large, elongated and un-refined grains could indicate that this was the original growth structure. If this is the case then it would suggest that competing anisotropies of some sort are still present at high undercoolings and that dendritic seaweed may be playing a crucial part in the spontaneous grain refinement process. However, access to higher undercoolings would be needed in order to investigate this further.

## 5. Conclusions

We have observed a number of microstructural transitions with increasing undercooling in a Cu-8.9wt%Ni alloy. At low undercooling, single grain droplets of <100> type dendrites give way to a recrystallised equiaxed grain structure, consistent with the low undercooling region of grain refinement observed in many alloys. At intermediate undercoolings, dendritic growth returns, consisting of dendrites of mixed <100> and <111> orientation. It is believed that this is an extended transition in growth orientation between fully <100> growth and fully <111> growth, with <111> character becoming more dominant as the undercooling is increased.

Competing anisotropies in the <100> and <111> growth directions appear to be giving rise to a novel form of the dendritic seaweed structure, characterised by its containment within a diverging split primary dendrite branch. Two types of this structure have been identified - <100> type and <111> type – the presence of which can be identified from the existence of weak background texture on the corresponding log-scale pole figures. At around $\Delta T = 200$ K, a positive break in the V-$\Delta T$ trend is observed, which is coincident with the transition to a large grained microstructure. We suggest that this break in the trend corresponds to the loss of all intermediate growth character and the transition to faster, fully <111> growth – though this is difficult to confirm microstructurally. At the highest undercoolings achieved, we observe an equiaxed-to-elongated grain structure which may be an intermediate structure in the spontaneous grain refinement phenomenon. Since some of the substructure observed is distinctly seaweed-like, we suggest that dendritic seaweed is assisting the spontaneous grain refinement process in some way.

## References


[1] Walker JL, editor The physical chemistry of process metallurgy. New York: Interscience, 1959.
[2] Kobayashi KF, Shingu PH. Journal of Materials Science 1988;23:2157.
[3] Cochrane RF, Battersby SE, Mullis AM. Materials Science and Engineering: A 2001;304-306:262.
[4] Battersby SE, Cochrane RF, Mullis AM. Materials Science and Engineering A 1997;226-228:443.
[5] Liu N, Yang G, Liu F, Chen Y, Yang C, Lu Y, Chen D, Zhou Y. Materials Characterization 2006;57:115.
[6] Tarshis LA, Walker JL, Rutter JW. Metallurgical Transactions 1971;2:2589.
[7] Li JF, Jie WQ, Yang GC, Zhou YH. Acta Materialia 2002;50:1797.
[8] Jackson KA, Hunt JD, Uhlmann DR, Seward TP. Trans. TMS-AIME 1966;236:149.
[9] Kattamis TZ, Flemings MC. Mod. Casting 1967;52.
[10] Schaefer RJ, Glicksman ME. Trans. AIME 1967;239:257.
[11] Schwarz M, Karma A, Eckler K, Herlach DM. Physical Review Letters 1994;73:1380.
[12] Karma A, Rappel W-J. Physical Review E 1998;57:4323.
[13] Mullis AM, Cochrane RF. International Journal of Non-Equilibrium Processing 2000;11:283.
[14] Mullis AM, Dragnevski KI, Cochrane RF. Materials Science and Engineering A 2004;375-377:157.
[15] Willnecker R, Herlach DM, Feuerbacher B. Physical Review Letters 1989;62:2707.
[16] Battersby SE, Cochrane RF, Mullis AM. Journal of Materials Science 1999;34:2049.
[17] Matson D. TMS. Warrendale, Pa: Minerals, Metals & Materials Society, 1998. p.233.
[18] Dragnevski KI, Cochrane RF, Mullis AM. Materials Science and Engineering A 2004;375-377:479.
[19] Sawada Y. Physica A: Statistical Mechanics and its Applications 1986;140:134.
[20] Gudgel KA, Jackson KA. Journal of Crystal Growth 2001;225:264.
[21] Dragnevski KI, Cochrane RF, Mullis AM. Metallurgical and Materials Transactions A 2004;35:3211.
[22] Algoso PR, Hofmeister WH, Bayuzick RJ. Acta Materialia 2003;51:4307.
[23] Boettinger WJ, Coriell SR, Trivedi R. Rapid solidification processing: principles and technologies. Baton Rouge (LA): Claitor's Publishing, 1988.
[24] Dantzig JA, Di Napoli P, Friedli J, Rappaz M. Metallurgical and Materials Transactions A 2013;Submitted.

**Figure Captions List:**

**Figure 1.** Growth velocity (V) as a function of undercooling (ΔT) and a summary of the growth transitions observed with increasing undercooling in Cu-8.9wt%Ni.

**Figure 2.** Micrograph of randomly-sectioned Cu-8.9wt%Ni droplet undercooled by ΔT = 35 K, taken in DIC mode to show coarse dendritic structure.

**Figure 3. (a)** Optical micrograph of Cu-8.9wt%Ni undercooled by ΔT = 65 K prior to nucleation in: bright field mode (top) where arrows show the positions of curved grain boundaries, and DIC mode (bottom) revealing a dendritic substructure which appears to cross the grain boundaries, as indicated by the arrows. The corresponding {200} pole figure is shown in **(b).**

**Figure 4. (a)** Optical through-focused micrograph and **(b)** SEM secondary electron image of the surface topography of a Cu-8.9wt%Ni droplet undercooled by ΔT = 139 K exhibiting an 8-fold nucleation pattern. Numbered features indicate (1) split primary dendrite trunk with orthogonal secondary branches (2) primary dendrite trunk with non-orthogonal <111> type branches (3) three seaweed branch structures of type (i) and (ii).

**Figure 5.** (Top) Showing pole figures corresponding to the ΔT = 139 K droplet shown in figure 6, (bottom) equivalent pole figures with intensity plotted on a log scale, the {111} plot showing two sets of poles with one pole shared between them, indicating twinned growth.

**Figure 6. (a)** Optical micrograph of the surface topography of a Cu-8.9wt%Ni droplet undercooled by ΔT = 161 K, exhibiting a 6-fold nucleation pattern (left) and corresponding {111} pole figure, with intensity plotted on a log scale (right). Numbered features indicate (1) primary dendrite branch exhibiting both orthogonal and non-orthogonal branches and (2) the branch of dendritic seaweed shown in **(b)** a montage SEM image of the full seaweed branch,

with nucleation point in the bottom, right-hand corner and the seaweed branch growing from right to left.

**Figure 7.** Cu-8.9wt%Ni sample undercooled by $\Delta T = 214$ K prior to nucleation **(a)** optical microscope image of the surface topography of the droplet showing an array of dendrites of mixed morphology and size and **(b)** a DIC micrograph of the of the droplet interior (left) showing coarse grains, whose underlying dendritic substructure appears to be discontinuous between neighbouring grains, and (right) the corresponding {111} pole figure.

**Figure 8**. Optical micrographs of a Cu-8.9wt%Ni droplet undercooled by $\Delta T = 220$ K, randomly sectioned and etched, showing **(a)** dark field montage image of the internal grain structure of the whole droplet and inset {111} pole figure. The area outlined indicates the approximate area depicted in **(b)** enhanced-contrast DIC micrograph showing the fine dendritic seaweed microstructure observed in this region.